



A Journal of the Gesellschaft Deutscher Chemiker

Angewandte Chemie

GDCh

International Edition

www.angewandte.org

Accepted Article

Title: Carrier-Free Delivery of Precise Drug-Chemogene Conjugates for Synergistic Treatment of Drug-Resistant Cancer

Authors: Lijuan Zhu, Yuanyuan Guo, Qihui Qian, Deyue Yan, Yuehua Li, Xinyuan Zhu, and Chuan Zhang

This manuscript has been accepted after peer review and appears as an Accepted Article online prior to editing, proofing, and formal publication of the final Version of Record (VoR). This work is currently citable by using the Digital Object Identifier (DOI) given below. The VoR will be published online in Early View as soon as possible and may be different to this Accepted Article as a result of editing. Readers should obtain the VoR from the journal website shown below when it is published to ensure accuracy of information. The authors are responsible for the content of this Accepted Article.

To be cited as: *Angew. Chem. Int. Ed.* 10.1002/anie.202006895

Link to VoR: <https://doi.org/10.1002/anie.202006895>

RESEARCH ARTICLE

Carrier-Free Delivery of Precise Drug-Chemogene Conjugates for Synergistic Treatment of Drug-Resistant Cancer

Lijuan Zhu,^{[a],[b]} Yuanyuan Guo,^[b] Qihui Qian,^[b] Deyue Yan,^{[a],[b]} Yuehua Li,^[c] Xinyuan Zhu,^[b] and Chuan Zhang^{*[b]}

- [a] Dr. L. Zhu, Prof. D. Yan
Institute of Molecular Medicine, Renji Hospital, School of Medicine, Shanghai Jiao Tong University
160 Pujian Road, Shanghai, 200217, China
- [b] Y. Guo, Q. Qian, Prof. D. Yan, Prof. X. Zhu, Prof. C. Zhang*
School of Chemistry and Chemical Engineering, Frontiers Science Center for Transformative Molecules, and State Key Laboratory of Metal Matrix Composites, Shanghai Jiao Tong University,
800 Dongchuan Road, Shanghai, 200240, China
E-Mail: chuanzhang@sjtu.edu.cn
- [c] Dr. Y. Li
Department of Radiology, Shanghai Jiao Tong University Affiliated Sixth People's Hospital, Shanghai Jiao Tong University School of Medicine
600, Yi Shan Road, Shanghai 200233, China
Supporting information for this article is given via a link at the end of the document.

Abstract: Combinatorial antitumor therapies using different chemodrug combo or chemo/gene agent combo emerge as promising ways to overcome the drug resistance, a major cause for the failure of cancer treatment. However, dramatic pharmacokinetic differences of adopted drugs greatly impede the combinatorial antitumor practices, raising the great demand of developing appropriate drug delivery systems (DDSs) for tumor treatment. By employing fluorescent dithiomaleimide (DTM) as a linker, herein, we conjugate two paclitaxel (PTX) molecules with a floxuridine (FdU)-integrated antisense oligonucleotide (termed as chemogene) to form a precise macromolecular drug-chemogene conjugate. This PTX-chemogene conjugate can self-assemble into spherical nucleic acid (SNA)-like micellular nanoparticle as a carrier-free DDS, which effectively knocks down the expression of P-glycoprotein first and subsequently releases the FdU and PTX to exert a synergistic antitumor effect and greatly inhibit the tumor growth. Our carrier-free DDS bearing drug/drug synergy and chemo/gene synergy may shed light on reversing multi-drug resistance of cancer.

Introduction

Multidrug resistance (MDR) greatly hinders the effectiveness of chemotherapy in cancer research and clinical applications, which are mainly caused by the adaptive gene expression of tumor cells under stressed pressure.^[1] For instance, P-glycoprotein (P-gp), a typical drug efflux pump that is usually overexpressed in drug-resistant cells, has proven to be a main factor to reduce the intracellular drug accumulation, especially for the hydrophobic drugs (e.g. vincristine, paclitaxel, doxorubicin), resulting in the failure of killing the tumor cells.^[2] To address this issue, two major strategies have been developed to reverse the drug resistance, including: combination use of different chemodrugs^[3] and synergistic administration of chemodrug/inhibitor combo.^[4] For the former case, different chemodrugs with diverse molecular mechanisms could exert antitumor effects cooperatively and improve the efficacy via preventing cancer cells to form compensatory resistance mechanism.^[5] For instance, combination use of doxorubicin and β -lapachone has been confirmed to against the drug-resistant breast tumor.^[6] However, the effectiveness of drug combination strategy is limited and

highly relies on the accurate molar ratio of the selected drugs.^[7] The latter approach involves the co-administration of chemodrug and drug resistance related protein inhibitors, such as small molecule inhibitors,^[8] antisense oligonucleotides (ASOs),^[9] small interfering RNAs,^[10] which restores the sensitivity of tumor cells to used chemodrug. As the drug resistance is mainly caused by the evolutionary adaption of tumor cells to the drug-induced pressure, reversing drug resistance at genetic level is more effective to treat the drug-resistant cancer. However, intrinsic differences between small molecular drugs and macromolecular gene therapeutics are even more prominent, making the delivery of chemodrug/gene combo more challenging. Although various materials, such as cationic polymers,^[11] micelles,^[12] liposomes,^[13] porous organic/inorganic nanomaterials,^[14] have been explored to serve as co-delivery carriers, concerns regarding drug loading capacity, stability, and biosafety remain in this field. As such, carrier-free DDS emerges as a new fashion in drug delivery study due to the avoidance of carrier-induced problems.^[15] For instance, amphiphilic drug-drug conjugate (ADDC)^[16] or amphiphilic supramolecular drug-drug (ASDD) pair^[17] have been engineered using two small molecular drugs with opposite solubility, which further self-assemble into micellular nanoparticles for systemic delivery. These strategies allow the delivery of selected drugs with accurate molar ratio to achieve great synergistic therapeutic effects, but usually with limited type of drug molecules. In contrast, carrier-free DDS containing both chemo and gene therapeutics is seldom explored so far.

Recently, we demonstrated a concept of chemogene that integrated chemodrug into sequence-specific nuclei acids to simultaneously perform as gene regulator and chemotherapeutic agents.^[18] However, chemogene alone is difficult to transfect the cells and play its functions owing to its negatively-charged feature, requiring us to construct a nanoformulation for delivery.^[18] Inspired by ADDC approach, we envision that conjugating a hydrophobic drug and chemogene to form a precise drug-chemogene conjugates (DCgCs) may not only overcome the carrier issue, but also achieve drug/drug and drug/gene combinatorial therapy to reverse the MDR. As a proof-of-concept, floxuridine (FdU) incorporated chemogene with antisense sequence that target P-gp gene is employed to conjugate with PTX to form the DCgC. As shown in Scheme 1, two PTX molecules are first connected to a fluorescent and azide-

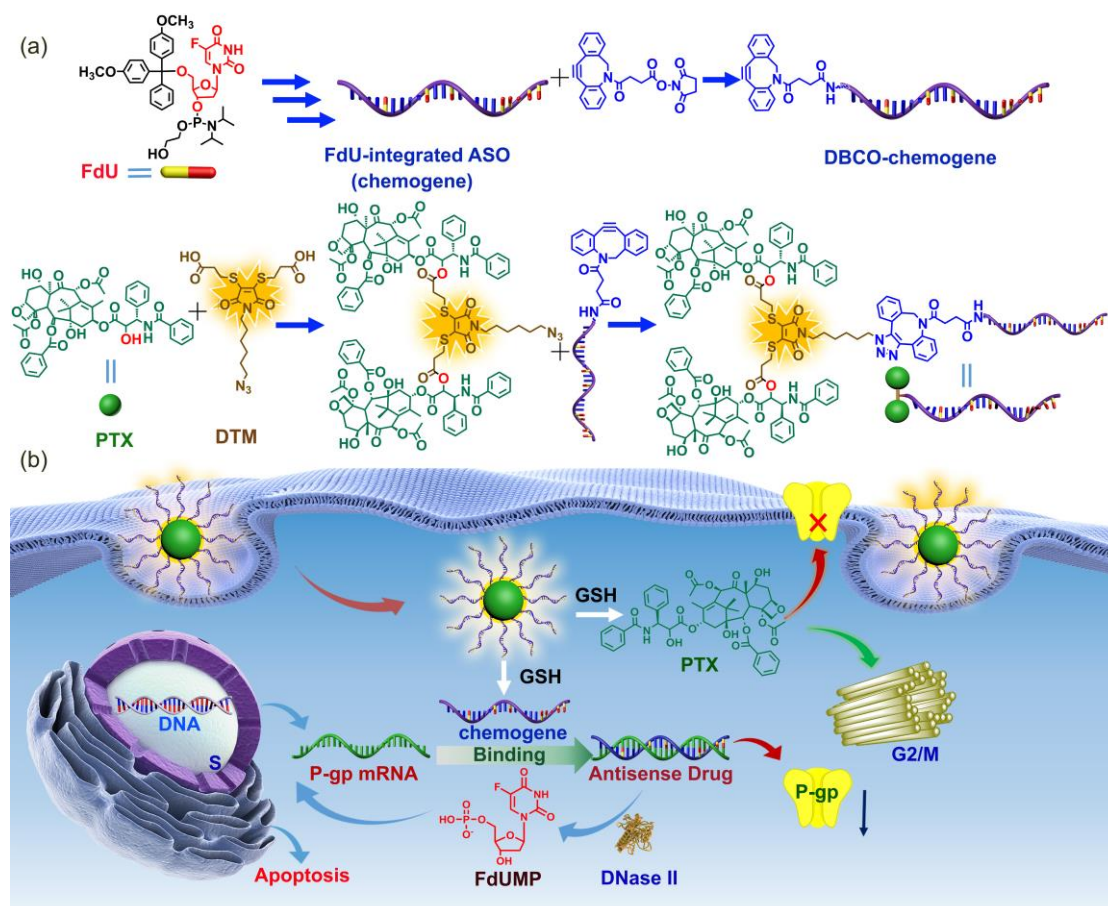
RESEARCH ARTICLE

containing DTM linker. Then the PTX dimer is further conjugated with chemogene through click chemistry. Owing to their amphiphilic feature, the obtained DCgCs can self-assemble into SNA-like micellar particles, which may exhibit improved physiological stability^[19] and high cellular transfection capability.^[20] Equipped with chemogene and PTX, the SNA-like assemblies first will knock down the P-gp expression, and then release the fluoride monophosphate (FdUMP) and PTX either by enzymatic degradation^[18,21] or glutathione reduction^[22], which can serve as active agents to synergistically inhibit the proliferation of tumor cells. With precise molecular design of DCgC and synergistic functions of its assembly, our carrier-free DDS exhibits great potential to reverse the drug resistance and suppress the growth of drug-resistant cancer.

Results and Discussion

First, the PTX-chemogene conjugate was synthesized as shown in Scheme 1a. In detail, PTX dimer with an azide group

was first synthesized by condensation of the fluorescent DTM and PTX with mole ratio of 1:2 (Figure S1 to S12). The successful synthesis of PTX dimer was confirmed by proton nuclear magnetic resonance (¹H-NMR, Figure S10), carbon nuclear magnetic resonance (¹³C-NMR, Figure S11) and Fourier-transform infrared spectroscopy (FTIR, Figure S12). Matrix-assisted laser desorption/ionization (Maldi-ToF) gave an m/z value at 2123.448, which could be attributed to [C₁₁₀H₁₂₀N₆O₃₂S₂+Na]⁺. Chemogene, anti-P-gp ASO, and scramble oligonucleotide (T20) with amine terminals (Table S1) were obtained by DNA solid-phase synthesis and further modified with dibenzocyclooctyne (DBCO) terminals via the reaction of amine and N-hydroxysuccinimide. 20% Denaturing polyacrylamide gel electrophoresis (PAGE, Figure S13) demonstrated the successful synthesis of the DBCO modified oligonucleotides. Then the PTX dimer with azide group was connected to the oligonucleotide strands by copper-free click chemistry. Maldi-ToF in Figure S14 verified the successful synthesis of PTX-chemogene.



Scheme 1. (a) The design and synthetic route of PTX-chemogene conjugates for the construction of self-fluorescent carrier-free DDS. (b) Schematic representation of PTX-chemogene assembly to reverse the drug resistance. SNA-like PTX-chemogene assembly could efficiently enter the cells and be degraded into PTX under intracellular GSH environment to prevent cell proliferation and chemogene to suppress the P-gp expression. Subsequently, FdUMP released by enzymatic degradation could further induce cancer cell apoptosis.

The obtained amphiphilic PTX-chemogene could self-assemble into nanoparticles in aqueous solution. After assembly, the product was verified by non-denaturing agarose gel electrophoresis (1% w/w). As shown in Figure 1a and Figure S15, a major sharp band with much lower mobility could be observed

on the gel for all PTX-conjugated oligonucleotides compared to that of free oligonucleotide strands, indicating the formation of large assembled structures with relatively narrow size distribution. To evaluate the stability of the obtained DDS, critical micelle concentrations (CMCs) of the PTX-oligonucleotide conjugates

RESEARCH ARTICLE

were determined by a previously reported method using Nile red as a fluorescent probe.^[23] The results showed that CMC values of assembled PTX-T20, PTX-ASO, and PTX-chemogene, were 8.7, 10.2, and 7.5 μM , respectively (Figure 1b). In addition, dynamic light scattering (DLS) measurements revealed that the average hydrodynamic diameters of micellar structures assembled by PTX-T20, PTX-ASO, and PTX-chemogene, were 89 nm, 105 nm, and 81 nm, with polydispersity index (PDI) of 0.172, 0.118, and 0.219, respectively (Figure 1c), which are suitable for systemic delivery.^[24] Meanwhile, cryogenic electron microscopy (Cryo-EM, Figure 1d), transmission electron microscopy (TEM, Figure S16 and Figure S17), and liquid atomic force microscopy (liquid AFM, Figure S18) showed that the self-assembled PTX-chemogene had spherical shape with the sizes ranging from ~ 50-90 nm. All these data revealed that the PTX-chemogene was successfully assembled into nanosized DDS.

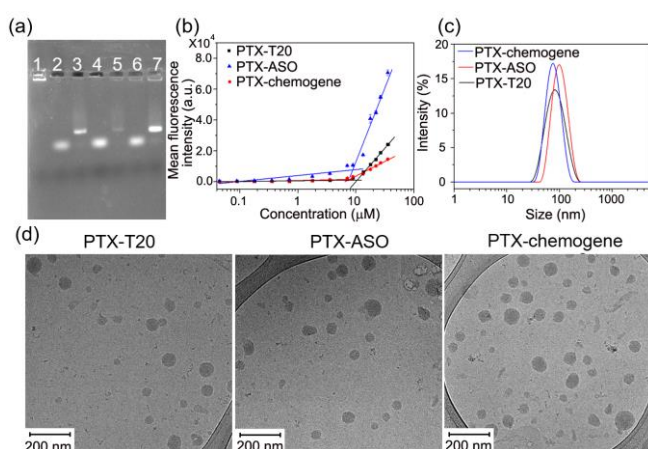


Figure 1. Characterizations of the SNA-like micellar particles assembled by PTX-T20, PTX-ASO, and PTX-chemogene conjugates. (a) Non-denaturing agarose gel (1% w/w) electrophoresis analysis of PTX dimer (lane 1), Anti-P-gp ASO (lane 2), PTX-ASO (lane 3), chemogene (lane 4), PTX-chemogene (lane 5), T20 (lane 6), PTX-T20 (lane 7). (b) The CMCs of PTX-T20, PTX-ASO, and PTX-chemogene determined by using Nile red as a fluorescence probe. (c) Hydrodynamic diameters of PTX-T20, PTX-ASO, and PTX-chemogene in aqueous solution. (d) Cryo-EM images of micellar particles assembled by PTX-T20, PTX-ASO, and PTX-chemogene (Scale bar: 200 nm).

DTM, produced by reaction of 2,3-dibromomaleimide and thiols, possesses a strong green fluorescence, which can be used for tracking the DDS.^[25] We used both flow cytometry and confocal laser scanning microscopy (CLSM) to evaluate the *in vitro* cellular uptake efficiency of PTX-chemogene using carboxyfluorescein (FAM) labeled free ASO as a control. As shown in Figure 2a, PTX-chemogene assembly showed an excitation wavelength of 405 nm and emission wavelength of 530 nm, which is similar to the fluorescence property of FAM-labeled ASO. Thus, PTX-chemogene assembly can perform as a self-fluorescent DDS for biomedical applications. Flow cytometry showed that the mean fluorescent intensity of PTX-chemogene assembly treated drug-resistant HeLa (HeLa/PTX) cells was over ten times higher than that of ASO/FAM treated group after 6 h incubation (Figure 2b), suggesting the rapid internalization of PTX-chemogene. Even after 6 h incubation, free DNA strands (ASO/FAM) still could hardly internalize the HeLa/PTX cells. Moreover, PTX-chemogene assembly treated HeLa/PTX cells exhibited stronger green fluorescence in the cytoplasm than that of ASO/FAM treated group after 2 h incubation as shown in Figure 2c. Both

flow cytometry and CLSM results indicated the efficient cellular uptake behavior of the obtained PTX-chemogene assembly, implying its potential to be an effective carrier for both chemodrugs and nucleic acid delivery.

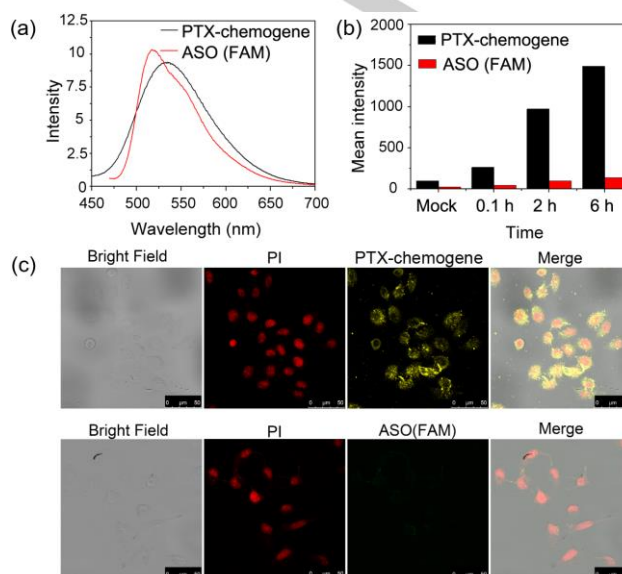


Figure 2. Self-fluorescent property of PTX-chemogene assemblies and their cellular uptake behaviour. (a) Fluorescence spectra of FAM-labelled anti-P-gp ASO (red line) and PTX-chemogene (black line). (b) Flow cytometry analysis of HeLa/PTX cells incubated with FAM-labelled free anti-P-gp ASO, and PTX-chemogene at the same oligonucleotide concentration of 2 μM at 37 $^{\circ}\text{C}$ for different time intervals, 0.1 h, 2 h, and 6 h respectively. (c) CLSM images of HeLa/PTX cells incubated with FAM-labelled free anti-P-gp ASO (yellow), and PTX-chemogene (yellow), at an oligonucleotides concentration of 2 μM at 37 $^{\circ}\text{C}$ for 2 h. Cell nuclei (red) were stained with PI. (Scale bar: 50 nm).

It has been widely reported that P-gp protein overexpressed on tumor cell membrane highly accounts for the reduction of intracellular drug accumulation and the raise of drug resistance for hydrophobic drugs.^[26] To investigate whether our designed PTX-chemogene assembly could reverse drug resistance through down regulating the P-gp protein expression, quantitative reverse transcription polymerase chain reaction (qRT-PCR) analysis and western blot assay were conducted to evaluate the P-gp expression at both mRNA and protein level. After treating with PTX-chemogene and a series of control samples, including naked ASO, PTX-T20 assembly, PTX-ASO assembly, and mock group, PTX-chemogene caused a 67% knockdown of P-gp mRNA in HeLa/PTX cells (Figure 3a), which was close to that induced by PTX-ASO (73%) and relative P-gp mRNA level in HeLa cells (87%). As a comparison, only 20% P-gp mRNA knockdown was observed in naked ASO, which could be ascribed to the poor cell uptake efficiency of naked DNA. Meanwhile, the P-gp mRNA knockdown of PTX-T20 assembly treated HeLa/PTX cells (34%) is much lower than those of PTX-chemogene and PTX-ASO treated cells, indicating that the anti-P-gp sequence was crucial to regulate the gene levels. Moreover, protein expression of P-gp valuated by western blot assay is consistent with the results of qRT-PCR analysis. P-gp protein expression was knocked down by 45% in PTX-chemogene treated HeLa/PTX cells, which is comparable to that of PTX-ASO treated cells (P-gp protein knockdown efficiency (46%)), as determined by band densitometry (Figure 3b). In contrast, PTX-T20 treated cells showed 20%

RESEARCH ARTICLE

reduction of P-gp expression, again demonstrating that the P-gp protein knockdown was sequence-specific. Meanwhile, free ASO strand failed to down regulate P-gp protein expression due to its poor cellular uptake. qRT-PCR and western blot results confirmed that PTX-chemogene could effectively knock down the target gene.

PTX-chemogene constructed through DTM bond, possesses a better thermal stability and reductive responsibility than disulfide bond bearing DDS.^[22] Owing to the differential concentration of glutathione tripeptide (GSH) between intracellular ($\sim 10^{-2}$ M) and extracellular microenvironment ($\sim 10^{-5}$ M),^[27] PTX-chemogene assembly could release PTX and chemogene after tumor cell uptake. The reduction responsive drug release behavior of PTX-chemogene assembly was evaluated under different conditions (1×PBS, pH 7.4, 0.5% w/v Tween 80, and with or without 10 mM dithiothreitol (DTT)) at 37 °C. Under PBS condition (pH 7.4, 0.5% w/v Tween 80) with 10 mM DTT, over 85% of PTX could be released from the PTX-chemogene assembly over 72 h (Figure S19). However, 10% PTX release was observed even after 72 h incubation without DTT treatment. Thereafter, MTT (3-(4,5-dimethylthiazol-2-yl)-2,5-diphenyl tetrazolium bromide) assay and cell apoptosis analysis were conducted to evaluate the antitumor effect of the new DDS using HeLa cells. As shown in Figure S20, the IC_{50} value of PTX-chemogene against HeLa cells (0.06 μ M) is much lower than that of PTX-ASO (0.16 μ M) and PTX-T20 (0.18 μ M), demonstrating the improved antitumor effect of chemo-gene synergistic therapy. Meanwhile, the IC_{50} value of free PTX against HeLa cells (0.03 μ M) was higher than that of mixture of PTX and FdU (0.02 μ M), which indicated that co-administration of PTX and FdU could efficiently improve the antitumor effect. However, IC_{50} value of PTX and chemogene mixture was 0.07 μ M, higher than that of PTX and FdU mixture, indicating the poor cell uptake of chemogene as illustrated above. In addition, enhanced cytotoxicity of the PTX-chemogene assembly was also confirmed by flow cytometry-based apoptosis assay (Figure S21).

A large number of previous studies have confirmed that down-regulation of drug-resistant related protein (P-gp) expression could effectively reverse cancer drug resistance. To evaluate whether our designed PTX-chemogene could reverse drug resistance and improve the anticancer efficacy in *in vitro* study, both MTT assay and cell apoptosis analysis were performed using HeLa/PTX cells. MTT assay showed that the increased cytotoxicity of PTX-chemogene (0.2 μ M) is comparable to that of PTX-ASO (2 μ M), which confirming the synergistic therapeutic effect of PTX and FdU (Figure 3c and 3d). Meanwhile, the cytotoxicity toward HeLa/PTX cells of PTX-ASO was 4-fold higher than that of PTX-T20, indicating that the antisense could specifically regulate protein expression and overcome the PTX resistance. Cell apoptosis assay showed that the total apoptosis rate of PTX-chemogene treated group is 77.2%, which is higher than that of PTX-ASO (54.7%) and PTX-T20 (39%, Figure S22). The results above demonstrated the higher cytotoxicity of PTX-chemogene, indicating that our new DDS indeed could effectively reverse the drug resistance. Importantly, the combination of PTX and FdU further improve the therapeutic efficacy.

Spherical nanoparticles with nanometer scale below 200 nm have been widely employed as DDSs due to the EPR effect.^[28] In this work, PTX-chemogene assembly with average hydrodynamic diameters of ~ 100 nm may have excellent EPR effect for *in vivo* experiments. To illustrate the bio-distribution of PTX-chemogene assembly, athymic nude mice bearing subcutaneous HeLa/PTX

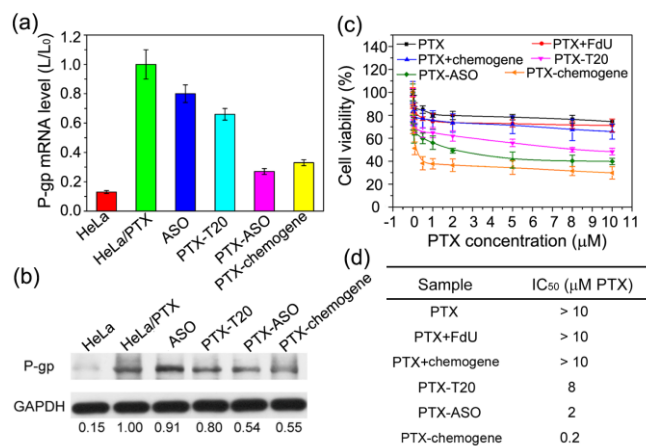


Figure 3. *In vitro* antitumor evaluation for the PTX-chemogene assembly. (a) P-gp mRNA expression in HeLa/PTX cells treated with different drug formulations, in which untreated HeLa and HeLa/PTX cells were used as controls. (b) Western blot image of P-gp protein expression in HeLa/PTX cells treated with different drug formulations. The relative intensity ratios of P-gp/GAPDH normalized to HeLa/PTX were marked. (c) *In vitro* antitumor effect of different drug formulations on HeLa/PTX cells evaluated by MTT assays. (d) Half maximal inhibitory concentration (IC_{50}) of different drug formulations for HeLa/PTX cell treatment.

tumors were subjected to *in vivo* optical imaging and an *ex vivo* bio-distribution study. Owing to the similar hydrodynamic diameter of PTX-ASO assembly and PTX-chemogene assembly, we investigated the bio-distribution of PTX-ASO assembly instead of PTX-chemogene assembly. Firstly, Cy5.5, Cy5.5-labeled ASO, and Cy5.5-labeled PTX-ASO assembly were intravenously injected into mice (100 μ g Cy5.5/kg mice). Then the whole-body optical imaging was applied at different post-injection time. As shown in Figure 4a, significant fluorescent signals were observed at the tumor site in PTX-ASO treated mice, which is much higher than that in naked ASO and free Cy 5.5 treated groups even after 8 h post-injection. To quantitatively analyze the bio-distribution of PTX-ASO assembly, the tumors and major organs were collected at 1 h, 4 h, 8 h, and 24 h post-injection and their fluorescence intensities were determined by *ex vivo* imaging (Figure 4c). Notably, PTX-ASO assembly showed 7 times higher tumor accumulation than those of naked ASO and free Cy5.5 after 1 h post-injection. Even after 8 h post-injection, the fluorescence intensity at the tumor site in PTX-ASO assembly treated group was still 5 times higher than that of naked ASO treated group. All these results above demonstrated that the PTX-ASO assembly had effective tumor accumulation effect due to the passive targeting effect.

To evaluate the *in vivo* antitumor efficacy of PTX-chemogene assemblies, athymic nude mice bearing drug-resistant HeLa tumors were intravenously administered with the self-assembled nanoparticles at a dose of PTX (8 mg/kg) once every 3 days. Meanwhile, PBS, free PTX, mixture of PTX and FdU, mixture of PTX and chemogene, PTX-T20, PTX-ASO with equivalent PTX dosage were used as controls. Tumor volume and body weight of all the treated mice were recorded before each administration to evaluate the *in vivo* treatment effect (Figure 5 and Figure S23). The tumor volume curves in Figure 5a showed that PTX-chemogene exhibited significant tumor growth inhibition. The average tumor volume of mice treated with PTX-chemogene was only 195 mm³ after 15 days treatment, which was much smaller

RESEARCH ARTICLE

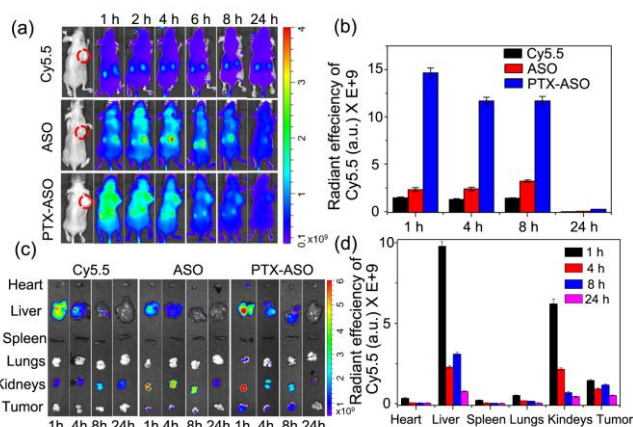


Figure 4. *In vivo* bio-distribution of PTX-ASO assembly in mice bearing subcutaneous HeLa/PTX tumors. The concentration of Cy5.5 injected was 100 $\mu\text{g}/\text{kg}$. (a) *In vivo* fluorescent imaging of the mice treated with free Cy5.5, Cy5.5-labeled ASO, and Cy5.5-labeled PTX-ASO assembly at 1 h, 2 h, 4 h, 6 h, 8 h, and 24 h post injection. Tumor sites are marked with red dashed circles. (b) Quantitative analysis of tumors distribution of free Cy5.5, Cy5.5-labeled ASO, and Cy5.5-labeled PTX-ASO assembly after 1 h, 4 h, 8 h, and 24 h injection. (c) Fluorescent images of different organs and tumors excised from the mice treated with different samples at different post-injection time, including 1 h, 4 h, 8 h, and 24 h respectively. (d) Quantitative accumulations of free Cy5.5, Cy5.5-labeled ASO, and Cy5.5-labeled PTX-ASO assemblies in major organs and tumors after 1 h, 4 h, 8 h, and 24 h injection.

than those treated with PTX-ASO (379 mm^3) and other control groups, demonstrating that co-delivery of PTX and FdU could improve the anti-cancer effect. Meanwhile, both PTX-chemogene and PTX-ASO showed better tumor inhibition effect on drug-resistant tumor than that of PTX-T20 (tumor volume: 623 mm^3), indicating that chemogene indeed reverse the drug resistance. However, the tumor volume of mice treated with PBS, free PTX, mixture of PTX and FdU, and mixture of PTX and chemogene increased quickly and reached to 885 mm^3 , 692 mm^3 , 637 mm^3 , and 541 mm^3 after 15 days treatment, respectively. This result indicated that free PTX did not show obvious therapeutic efficiency on drug-resistant tumor, while the co-administration of PTX and chemogene could partially reverse the drug resistance and slightly retard the tumor growth.

After the 15 days treatment, all treated mice were sacrificed and then the tumors were photographed (Figure 5b). The tumor inhibitory rate (TIR) calculated from tumor weight showed that PTX-chemogene treated group appeared the highest inhibition rate, 80% inhibition rate compared to that of PBS treated group (Figure 5c). Histology and immunofluorescence analysis of tumors dissected from different formulation treated mice were conducted to further evaluate the antitumor efficacy after treatments (Figure S24). The hematoxylin and eosin (H&E) staining results showed that the tumor cells of PBS treated group presented large nucleus (blue), suggesting a rapid tumor cell growth of none drug treated group. In contrast, PTX-chemogene and PTX-ASO treated group appeared obvious small nuclear fragments and nuclear shrinkage, indicating the apoptosis of tumor tissues. Furthermore, necrotic areas were apparently observed in both PTX-chemogene and PTX-ASO treated group. However, H&E staining images of tumors treated with mixture of PTX and FdU or mixture of PTX and chemogene appeared a small number of vacuolization and apoptotic areas, which indicated that combined chemo-drug administration could partially

enhance the anti-cancer effect on drug-resistant cancers. Meanwhile, ki67 antigen expression implied that PTX-chemogene could effectively inhibit the proliferation of cancer cells. Besides, terminal deoxynucleotidyl transferase-mediated dUTP nick-end labeling (TUNEL) assay was further carried out to evaluate the cell apoptosis in tumor tissues. From the TUNEL results, PTX-chemogene assembly was the most effective pathway to induce tumor cell apoptosis among all the other therapeutics, which is corresponding to the results of H&E staining. Immunohistochemical analysis in Figure S24 illustrated that PTX-chemogene assembly could dramatically suppressed P-gp protein expression in *in vivo* study. To further quantitatively confirm the *in vivo* P-gp regulation of PTX-chemogene, qRT-PCR and western blot assay were used to analyze the P-gp gene and protein expression levels of tumors treated with different formulations, respectively. As shown in Figure 5d and 5e, PTX-chemogene down-regulated 67% of P-gp mRNA and 86% of P-gp protein, using GAPDH as an internal control, which were equivalent to those of PTX-ASO (73% knockdown of P-gp gene and 90% knockdown of P-gp protein). These results showed that FdU integrated ASO did not affect the performance of ASO.

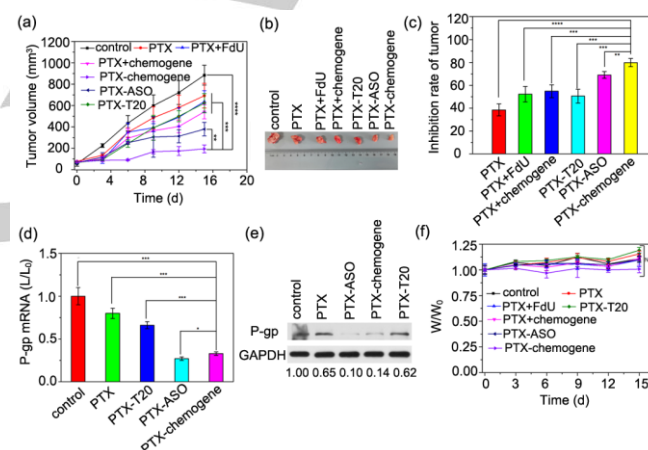


Figure 5. *In vivo* anticancer effect and gene regulation of PTX-chemogene assembly in mice bearing HeLa/PTX tumors. PTX, PTX+FdU, PTX+chemogene, PTX-T20, PTX-ASO, and none treated group were used as controls. (a) Changes of tumor growth volume after intravenous injection of different formulations in HeLa/PTX tumor-bearing nude mice ($n = 4$ in each group, concentration of PTX: 8 mg/kg). (b) Images of tumors exciliated from mice in each group after 15 days treatment. (c) Tumor inhibitory rate (TIR) after treatment. ($n = 4$). (d) P-gp mRNA levels of different formulations treated drug resistant tumors (L) compared to none-treated group (L_0). (e) P-gp protein expression of different formulations treated drug-resistant tumors. (f) Body weight changes of HeLa tumor-bearing mice after treatment with PBS, PTX, PTX+FdU, PTX+chemogene, PTX-T20, PTX-ASO, and PTX-chemogene. Statistical significance: **** $P < 0.0001$, *** $P < 0.001$, ** $P < 0.01$, * $P < 0.1$, NS no significant difference.

At the meantime, no significant changes in body weight of mice in all treated group could be observed, implying the bio-safety of PTX-chemogene assembly (Figure 5f). Otherwise, blood biochemical indicators of PTX-chemogene treated mice did not show obvious hepatic and renal toxicity (Figure S25). Histological examination of organs (heart, liver, spleen, lungs, and kidneys) displayed no obvious tissue destruction, apoptosis, or inflammation on morphology, which ensured the biosafety of PTX-chemogene (Figure S26). These results demonstrated that the PTX-chemogene assemblies could effectively induce the

RESEARCH ARTICLE

apoptosis of tumor tissue without causing systemic toxicity on other organs at the therapeutic dosage.

Conclusion

In summary, we reported a new carrier-free DDS assembled by precise drug-chemogene conjugates, which integrates combinatorial chemodrug therapy and chemo/gene therapy to treat the drug-resistant tumor. PTX and FdU-integrated chemogene were conjugated by fluorescent DTM linker without employing any exogenous carriers. The molar ratio of PTX, FdU and chemogene could be precisely controlled through well-established solid-phase synthesis and click conjugation. With an amphiphilic design, the obtained PTX-chemogene conjugates could further assemble into SNA-like micellar nanoparticles with high cellular uptake efficiency. Upon internalizing into the cancer cells, the high concentration of intracellular GSH environment triggered the release of chemogene to knockdown the P-gp expression (up to 73%) and PTX to induce the cell apoptosis. The FdUMP subsequently released by enzymatic degradation could further prevent proliferation of the cancer cells, achieving a synergistic antitumor effect with a inhibit rate against drug-resistant tumor up to ~ 80%. Compared to carrier-based DDSs, our drug conjugate design is precise and simple, which could be easily expanded to integrate other types of therapeutics. For instance, nucleic acid analogues rather than FdU could be similarly integrated into the chemogenes and their sequences can also be selected to target many other genes. This method provides a new pathway for tumor therapy.

Acknowledgements

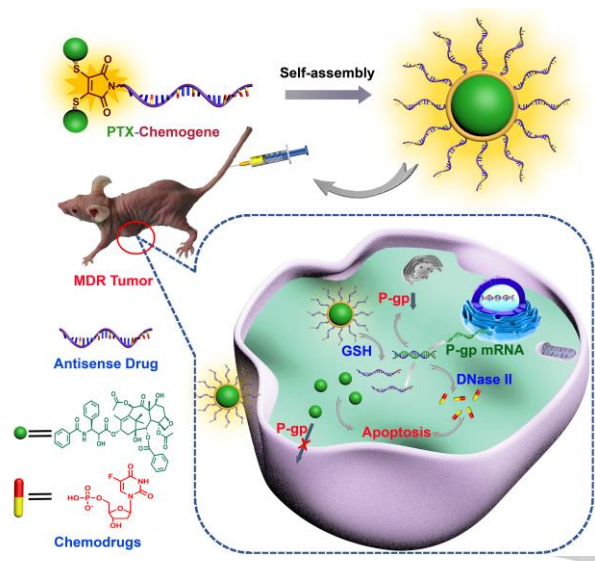
This work was financially supported by the National Key Research and Development Program of China (2018YFC1106100, 2018YFC1106102, 2018YFA0902600), the National Natural Science Foundation of China (21805129, 21661162001, 21673139, 51973112, 51690151, 81671673, 81871329).

Keywords: drug resistance • chemotherapy • gene therapy • nucleoside analogue • chemogene

- [1] a) C. Holohan, S. Van Schaeybroeck, D. B. Longley, P. G. Johnston, *Nat. Rev. Cancer* **2013**, *13*, 714-726. b) G. Szakacs, J. K. Paterson, J. A. Ludwig, C. Booth-Genthe, M. M. Gottesman, *Nat. Rev. Drug Discov.* **2006**, *5*, 219-234. c) S. Agnello, M. Brand, M. F. Chellat, S. Gazzola, R. Riedl, *Angew. Chem. Int. Ed.* **2018**, *58*, 3300-3345.
- [2] a) M. M. Lee, Z. Gao, B. R. Peterson, *Angew. Chem. Int. Ed.* **2017**, *56*, 6927-6931. b) C. Chen, J. E. Chin, K. Ueda, D. P. Clark, I. Pastan, M. M. Gottesman, I. B. Roninson, *Cell* **1986**, *47*, 381-389. c) J. I. Fletcher, M. Haber, M. J. Henderson, M. D. Norris, *Nat. Rev. Cancer* **2010**, *10*, 147-156.
- [3] a) X. Liang, C. Gao, L. Cui, S. Wang, J. Wang, Z. Dai, *Adv. Mater.* **2017**, *29*, 1703135. b) X. Wei, Y. Wang, X. Xiong, X. Guo, L. Zhang, X. Zhang, S. Zhou, *Adv. Funct. Mater.* **2016**, *26*, 8266. c) Y. Xiao, J. Liu, M. Guo, H. Zhou, J. Jin, J. Liu, Y. Liu, Z. Zhang, C. Chen, *Nanoscale* **2018**, *10*, 12639-12649.
- [4] a) P. Huang, G. Wang, Y. Su, Y. Zhou, W. Huang, R. Zhang, D. Yan, *Theranostics* **2019**, *9*, 5755-5768. b) J. Liu, L. Song, S. Liu, S. Zhao, Q. Jiang, B. Ding, *Angew. Chem. Int. Ed.* **2018**, *57*, 15486-15490. c) C. He, K. Lu, D. Liu, W. Lin, *J. Am. Chem. Soc.* **2014**, *136*, 5181-5184.
- [5] a) J. R. Pritchard, D. A. Lauffenburger, M. T. Hemann, *Drug Resist. Updat.* **2012**, *15*, 249-257. b) W. F. Mangel, W. J. McGrath, M. T. Brown, M. L. Baniecki, D. L. Barnard, Y. P. Pang, *Curr. Med. Chem.* **2001**, *8*, 933-939.
- [6] M. Ye, Y. Han, J. Tang, Y. Piao, X. Liu, Z. Zhou, J. Gao, J. Rao, Y. Shen, *Adv. Mater.* **2017**, *29*, 1702342.
- [7] P. G. Tardi, R. C. Gallagher, S. Johnstone, N. Harasym, M. Webb, M. B. Bally, L. D. Mayer, *Biochim. Biophys. Acta, Gen. Subj.* **2007**, *1768*, 678-687.
- [8] a) J. Tang, L. Zhang, H. Gao, Y. Liu, Q. Zhang, R. Ran, Z. Zhang, Q. He, *Drug Deliv.* **2016**, *23*, 1130-1143. b) X. Duan, J. Xiao, Q. Yin, Z. Zhang, H. Yu, S. Mao, Y. Li, *ACS Nano* **2013**, *7*, 5858-5869.
- [9] X. Li, A. P. Smyth, D. J. Barrett, S. P. Ivy, E. von Hofe, *Leukemia* **1997**, *11*, 950-957.
- [10] a) M. Zheng, T. Jiang, W. Yang, Y. Zou, H. Wu, X. Liu, F. Zhu, R. Qian, D. Ling, K. McDonald, J. Shi, B. Shi, *Angew. Chem. Int. Ed.* **2019**, *58*, 4938-4942. b) X. B. Xiong, A. Lavasanifar, *ACS Nano* **2011**, *5*, 5202-5213.
- [11] Z. Ye, W. R. Wu, Y. F. Qin, J. Hu, C. Liu, P. H. Seeberger, J. Yin, *Adv. Funct. Mater.* **2018**, *28*, 1706600.
- [12] X. Tan, X. Lu, F. Jia, X. Liu, Y. Sun, J. K. Logan, K. Zhang, *J. Am. Chem. Soc.* **2016**, *138*, 10834-10837.
- [13] O. B. Garbuzenko, M. Saad, V. P. Pozharov, K. R. Reuhl, G. Mainelis, T. Minko, *Proc. Natl Acad. Sci. USA* **2010**, *107*, 10737-10742.
- [14] B. Liu, F. Hu, J. Zhang, C. Wang, L. Li, *Angew. Chem. Int. Ed.* **2019**, *58*, 8804-8808.
- [15] S. Y. Qin, A. Q. Zhang, S. X. Cheng, L. Rong, X. Z. Zhang, *Biomaterials* **2017**, *112*, 234-247.
- [16] a) P. Huang, D. Wang, Y. Su, W. Huang, Y. Zhou, X. Zhu, D. Yan, *J. Am. Chem. Soc.* **2014**, *136*, 11748-11756. b) W. Lin, T. Sun, Z. Xie, J. Gu, X. Jing, *Chem. Sci.* **2016**, *7*, 1846-1852.
- [17] a) Z. Zhang, L. Shi, C. Wu, Y. Su, J. Qian, H. Deng, X. Zhu, *ACS Appl. Mater. Inter.* **2017**, *9*, 29505-29514. b) R. Zhang, R. Xing, T. Jiao, K. Ma, C. Chen, G. Ma, X. Yan, *ACS Appl. Mater. Inter.* **2016**, *8*, 13262-13269. c) L. P. Zhao, R. R. Zheng, H. Q. Chen, L. S. Liu, X. Y. Zhao, H. H. Liu, X. Z. Qiu, X. Y. Yu, H. Cheng, S. Y. Li, *Nano Lett.* **2020**, *20*, 2062-2071.
- [18] Q. Mou, Y. Ma, F. Ding, X. Gao, D. Yan, X. Zhu, C. Zhang, *J. Am. Chem. Soc.* **2019**, *141*, 6955-6966.
- [19] a) D. S. Seferos, A. E. Prigodich, D. A. Giljohann, P. C. Patel, C. A. Mirkin, *Nano Lett.* **2009**, *9*, 308-311. b) A. E. Prigodich, A. H. Alhasan, C. A. Mirkin, *J. Am. Chem. Soc.* **2011**, *133*, 2120-21123.
- [20] a) S. Zhu, H. Xing, P. Gordiichuk, J. Park, C. A. Mirkin, *Adv. Mater.* **2018**, *30*, 1707113. b) C. H. J. Choi, L. Hao, S. P. Narayan, E. Auyeung, C. A. Mirkin, *Proc. Natl Acad. Sci. USA* **2013**, *110*, 7625-7630.
- [21] a) Q. Mou, Y. Ma, G. Pan, B. Xue, D. Yan, C. Zhang, X. Zhu, *Angew. Chem. Int. Ed.* **2017**, *56*, 12528-12532. b) Y. Ma, H. Liu, Q. Mou, D. Yan, X. Zhu, C. Zhang, *Nanoscale* **2018**, *10*, 8367-8371.
- [22] a) H. Wang, M. Xu, M. Xiong, J. Cheng, *Chem. Commun.* **2015**, *51*, 4807-4810. b) X. Guo, L. Wang, K. Duval, J. Fan, S. Zhou, Z. Chen, *Adv. Mater.* **2018**, *30*, 1705436. c) M. W. Jones, R. A. Strickland, F. F. Schumacher, S. Caddick, J. R. Baker, M. I. Gibson, D. M. Haddleton, *J. Am. Chem. Soc.* **2012**, *134*, 1847-1852.
- [23] E. Chevallier, C. Monteux, F. Lequeux, C. Tribet, *Langmuir* **2012**, *28*, 2308-2312.
- [24] a) A. Albanese, P. S. Tang, W. C. W. Chan, *Annu. Rev. Biomed. Eng.* **2012**, *14*, 1-16. b) H. Kobayashi, R. Watanabe, P. L. Choyke, *Theranostics* **2014**, *4*, 81-89.
- [25] a) M. P. Robin, R. K. O'Reilly, *Chem. Sci.* **2014**, *5*, 2717-2723. b) M. P. Robin, P. Wilson, A. B. Mabire, J. K. Kiviho, J. E. Raymond, D. M. Haddleton, R. K. O'Reilly, *J. Am. Chem. Soc.* **2013**, *135*, 2875-2878. c) M. E. B. Smith, F. F. Schumacher, C. P. Ryan, L. M. Tedaldi, D. Papaioannou, G. Waksman, S. Caddick, J. R. Baker, *J. Am. Chem. Soc.* **2010**, *132*, 1960-1965.
- [26] W. Keller, R. Crouch, *Proc. Natl Acad. Sci. USA* **1972**, *69*, 3360-3364.
- [27] a) T. B. Ren, Y. Feng, Z. H. Zhang, L. Li and Y. Y. Li, *Soft Matter*, **2011**, *7*, 2329-2331. b) F. Q. Schafer, G. R. Buettner, *Free Radical Biol. Med.* **2001**, *30*, 1191-1212.
- [28] a) V. Torchilin, *Adv. Drug Deliver. Rev.* **2011**, *63*, 131-135. b) H. Maeda, J. Wu, T. Sawa, Y. Matsumura, K. Hori, *J. Control. Release* **2011**, *65*, 271-284.

RESEARCH ARTICLE

Entry for the Table of Contents



A carrier-free drug delivery system is assembled by a precise amphiphilic drug-chemogene conjugate, which is prepared by conjugating two paclitaxel molecules with an floxuridine-integrated antisense using a fluorescent dibromomaleimide linker. With two component chemodrugs bearing synergistic antitumor effect and antisense sequence to knock down the P-glycoprotein, our PTX-chemogene assembly can effectively reverse drug resistance and inhibit the tumor growth.